A Godunov Method for Supersonic Tactical Missiles

A.B. Wardlaw Jr.,* F.P. Baltakis,† F.M. Martin,‡
F.J. Priolo,§ and R.U. Jettmar§
Naval Surface Weapons Center, Silver Spring, Maryland

This paper describes a Godunov method applicable to tactical missiles in steady supersonic flow. The scheme is cast in a finite-volume formulation using a mesh generated by a multiple-zone procedure. The bow shock is fitted using the information contained in the Riemann problem. Surface pressures are determined using a method of characteristics analysis that degenerates near shocks or expansions to the oblique shock or Prandtl-Meyer expansion relations. The scheme is applied to body-alone and finned configurations and calculations are completed without the use of artificial viscosity or special procedures.

Nomenclature

A^n	= area of control volume edge lying in the $z = z^n$ plane
$b(\phi,z)$	= radial position of edge 3 (see Fig. 2)
$c(\phi,z)$	= radial position of edge 1 (see Fig. 2)
C_N	= normal force
F	= flux vector [Eq. (7)]
H_0	= stagnation enthalpy
$n = (n_x,n_y,n_z)$	= vector normal to cell edge; $\|n\|$ = edge area
p	= pressure
(r,ϕ,z)	= cylindrical coordinates (Fig. 2)
U	= flux vector [(Eq. (7)].
(u,v,w)	= Cartesian velocity components
v_n	= velocity component normal to cell edge
v_t	= velocity component tangent to cell edge
(x,y,z)	= Cartesian coordinates where z is along the missile axis
$z_{c.p.}$	= center of pressure
γ	= ratio of specific heats
δ	= flow direction angle
(ξ,η,ζ)	= computational coordinates
$\sigma(r,z)$	= angular location of edge 4 (see Fig. 2)
$\psi(r,z)$	= angular location of edge 2 (see Fig. 2)

Subscripts

$\pm$	= upper and lower Riemann states (see Fig. 3)
c	= at a point on a characteristic
f	= on the slip line of the Riemann problem
w	= at a wall point
∞	= ambient condition

Superscript

$(\tilde{\ })$	= average property along a cell edge

Received July 15, 1985; presented as Paper 85-1812 at the AIAA Atmospheric Flight Mechanics Conference, Snowmass, CO, Aug. 19-21, 1985; revision received Jan. 16, 1986.

*Aerospace Engineer, Applied Mathematics Branch. Associate Fellow AIAA.
†Aerospace Engineer, Aerodynamics Branch. Member AIAA.
‡Mechanical Engineer, Systems Analysis Branch.
§Aerospace Engineer, Applied Mathematics Branch. Member AIAA.

Introduction

THIS paper investigates application of a finite volume Godunov method to steady supersonic flow, with the objective of producing a more robust computational method. The Godunov scheme was originally proposed for unsteady gasdynamics, but can easily be extended to steady supersonic flow. Unlike conventional numerical schemes that presume a smooth flowfield, the Godunov method assumes that the flowfield consists of a number of piecewise constant states with discontinuities occurring midway between the mesh points. The evolution of the flowfield in the vicinity of the discontinuities is determined by solving the associated Riemann problem. The resulting method is first-order accurate, but can be extended to higher order.[1]

Computational methods are currently available for calculating inviscid supersonic flow about arbitrary bodies. Such techniques take advantage of the hyperbolic nature of the supersonic Euler equations and march a known cross-flow data plane down the length of a missile. Traditional methods for solving the Euler equations use complicated transformations to treat finned shapes[2-8] and are difficult to apply to geometries with sharp wing edges. An alternative approach using a multiple-zone strategy has been developed in Refs. 9 and 10. Here the cross section is divided into several zones, each of which can be treated with a simple transformation.

These methods are based on MacCormack's explicit scheme, which is second-order accurate, and apply a special analysis at the fin edges. Although this type of approach is being widely used, it is not particularly robust and artificial viscosity and special differencing procedures must often be applied to complete a calculation. The amount of artificial viscosity to be used, as well as the fin tip differencing strategy, must be determined on a trial-and-error basis.

This paper describes a numerical procedure, based on Godunov's first-order method that is sufficiently robust to handle body/wing geometries without the explicit addition of artificial viscosity or special procedures. This method is cast within a simplified multiple zone framework and is capable of treating conventional missile shapes. It is applied to body-alone, body/wing, and body/wing/tail configurations.

Solution Methodology

The Godunov's scheme is cast in a finite-volume formulation that removes corner and fin-tip points arising in the analogous finite-difference, mutliple-zone formulation. This significantly simplifies the boundary treatment by eliminating the need for special analysis at these points.

Mesh Generation

The computation scheme uses a multiple-zone approach that provides a convenient framework from which to compute finned bodies with sharp fin edges. This entails dividing the cross-flow plane up into several zones and applying a simple, separate mapping to each zone. Zone boundaries are taken to coincide with body, fin, or tail surfaces and the bow shock. A sample multiple zone grid for a finned missile configuration is illustrated in Fig. 1. Location of a mesh boundary at the bow shock is not essential, since Godunov's method is sufficiently robust to capture the bow shock. However, it improves computational efficiency by restricting the size of the computational domain to the estimated shock-layer region.

Each zone consists of a generalized quadrilateral region as shown in Fig. 2. For missiles with circular bodies, cylindrical coordinates are generally used: the radial locations of edges 1 and 3 are described in terms of the functions $b(\phi,z)$ and $c(\phi,z)$, while the angular position of edges 2 and 4 are defined by $\psi(r,z)$ and $\sigma(r,z)$. The transformation is divided into two parts: $T=T_1T_2$ where T_2: $(r,\phi,z)\rightarrow(x,y,z)$ and T_1: $(\xi,\eta,\zeta)\rightarrow(r,\phi,z)$. Within computational space, $0\le\xi\le1$, $0\le\eta\le1$, and $\zeta\ge0$. T_2 is defined analytically, while T_1 is determined as follows:

$$r=b(\phi',\zeta)+[c(\phi'',\zeta)-b(\phi',\zeta)]F(\xi)$$

$$\phi=\sigma(r',\zeta)+[\psi(r'',\zeta)-\sigma(r',\zeta)]G(\eta)$$

$$z=\zeta \tag{1}$$

where

$$\phi'=\phi_4(\zeta)+[\phi_1(\zeta)-\phi_4(\zeta)]G(\eta)$$

$$\phi''=\phi_3(\zeta)+[\phi_2(\zeta)-\phi_3(\zeta)]G(\eta)$$

$$r'=r_4(\zeta)+[r_3(\zeta)-r_4(\zeta)]F(\xi)$$

$$r''=r_1(\zeta)+[r_2(\zeta)-r_1(\zeta)]F(\xi)$$

Here F and G are clustering functions in ξ and η, with $F(0)=G(0)=0$ and $F(1)=G(1)=1$, while (r_i,ϕ_i) are the coordinates of corner i, $i=1$-4.

The Riemann Problem

In steady supersonic flow, the Riemann problem represents the confluence of two two-dimensional supersonic streams, as is illustrated in Fig. 3. At the point of stream intersection, shocks or expansion fans form to turn both streams to a common direction. The appropriate direction is the one producing the same pressure in both streams. The two final streams need not feature the same density or velocity and, in fact, a slip line generally forms between them. The resulting solutions are self-similar in z and feature constant properties along any line passing through the point of initial stream intersection.

Figure 3 depicts a Riemann problem formed by the intersection of two streams with properties (p_+,ρ_+,u_+,w_+) and (p_-,ρ_-,u_-,w_-). Upward deflection of the (+) stream is described by the shock relations and leads to an increase in pressure, while downward deflection is associated with an expansion and leads to a decrease in pressure. On the other hand, upward deflection of the (−) stream leads to an expansion and downward deflection to a shock. To solve the Riemann problem, it is necessary to determine the final flow direction that produces the same final pressure in both streams. The shock and expansion equations define the relation between the two initial flow directions $\delta_\pm$, pressure $p_\pm$ and final pressure and direction p_f, δ_f. These can be written expressing δ_f as a function of $\delta_\pm$, $p_\pm$, and p_f as

$$\delta_f=\delta_\pm\pm\tan^{-1}\left[\left(\frac{(p_f-p_\pm)}{(\gamma M_\pm+1)p_\pm-p_f}\right)^2\times\left(\frac{p_\pm(2\gamma M_\pm^2-\gamma+1-(\gamma+1)p_f}{(\gamma+1)p_f+(\gamma-1)p_\pm}\right)\right]^{1/2}\quad\text{shock } p_f>p_\pm \tag{2}$$

$$\delta_f=\delta_\pm\pm\nu(M_\pm)\mp\nu(M_f)\qquad\text{expansion } p_f<p_\pm \tag{3}$$

where

$$M_f=\left\{\frac{2}{(\gamma-1)}\left[\left(\frac{p_\pm}{p_f}\right)^{(\gamma-1)/\gamma}\left(1+\frac{(\gamma-1)}{2}M_\pm^2\right)-1\right]\right\}^{1/2}$$

$$\nu(M)=\tilde{C}\tan^{-1}\left[\frac{(M^2-1)}{\tilde{C}}\right]^{1/2}-\tan^{-1}[M^2-1]^{1/2}$$

$$\tilde{C}=\left[\frac{(\gamma+1)}{(\gamma-1)}\right]^{1/2}$$

Here the upper and lower signs are associated with the (+) and (−) streams, respectively. The nonlinearity of these relations precludes a closed-form solution (the details of an iterative procedure, based on the secant method, are given in Ref. 1).

Fortunately, the complete Riemann problem need not be solved in most cases. In smooth-flow regions, property variations between adjacent cells are small and approximate closed-form solutions can be obtained. Equations (2) and (3) can be expanded in a Taylor series for $|\delta-\delta_\pm|\ll1$.[11] Retaining only the linear terms yields

$$\delta_f=\delta_\pm\pm\frac{(p_f-p_\pm)}{\kappa_\pm}$$

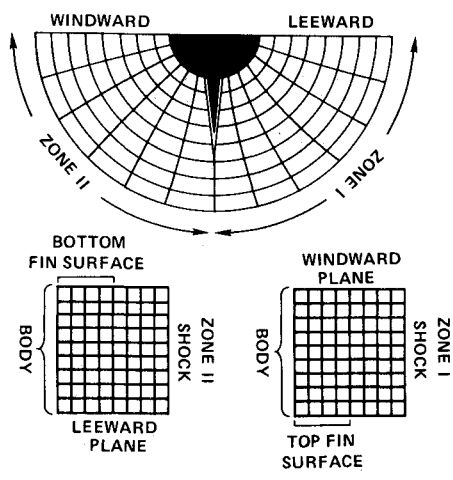

Fig. 1 Multiple zone mesh.

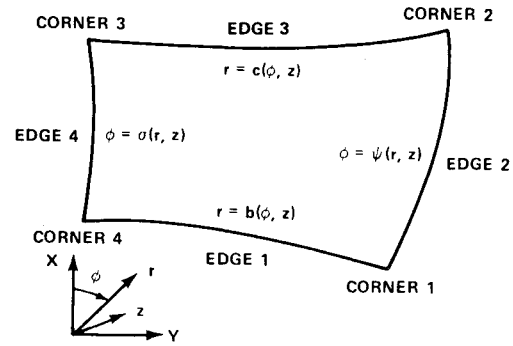

Fig. 2 Generalized quadrilateral zone structure.

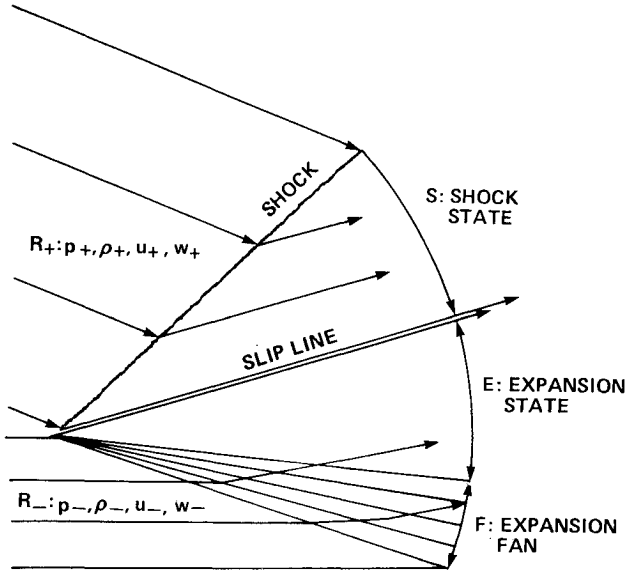

Fig. 3 The supersonic Riemann problem consists of two intersecting supersonic streams, R_+, and R_-.

where

$$\kappa_\pm = \gamma M_\pm^2 p_\pm / (M_\pm^2 - 1)^{1/2} \tag{4}$$

Simultaneous solution of the (+) and (−) stream equations produces the linear Riemann problem solution,

$$\tilde{p}_f = p_+ + \frac{\kappa_+ [(p_- - p_+) + \kappa_- (\delta_- - \delta_+)]}{(\kappa_+ + \kappa_-)} \tag{5a}$$

$$\tilde{\delta}_f = \delta_+ + \frac{[(p_- - p_+) + \kappa_- (\delta_- - \delta_+)]}{(\kappa_+ + \kappa_-)} \tag{5b}$$

This solution is used if $|\delta_\pm - \tilde{\delta}_f| < 0.01$. For problems not meeting this criterion, second- and third-order terms are added and in extreme cases Eqs. (2) and (3) can be solved iteratively.

The Godunov procedure, which is described below, requires knowledge of the flow properties associated with a specific direction θ. As indicated in Fig. 3, three different regions $(R_\pm, F, E)$ are featured on the expansion side of a slip line and two $(R_\pm, S)$ on the shock side. Here $R_\pm$ are the original states, S and E the regions behind a shock or expansion, and F the expansion fan. If θ lies in $R_\pm$, the initial conditions provide the needed properties. For θ lying in S or E, the variables p and δ are determined by the Riemann solution, and the density is computed using the oblique shock relations. In region E, the isentropic relation provides the correct density; however, the shock relation is less expensive to apply and yields the required accuracy, except behind severe expansions. When θ lies in region F, properties can be calculated by noting that the flow direction δ along θ is given by

$$\delta = \theta \mp \sin^{-1}\{1/M^*\}$$

where M^* is the Mach number along the direction θ. Using Eq. (3)

$$\delta_\pm \pm \nu(M_\pm) = \theta \pm \nu(M^*) \mp \sin^{-1}\{1/M^*\}$$

and solving for M^* yields

$$M^* = \left\{1 + \tilde{C}^2 \tan^2\left[\frac{\pi/2 + \nu(M_\pm) \pm (\delta_\pm - \theta)}{\tilde{C}}\right]\right\}^{1/2}$$

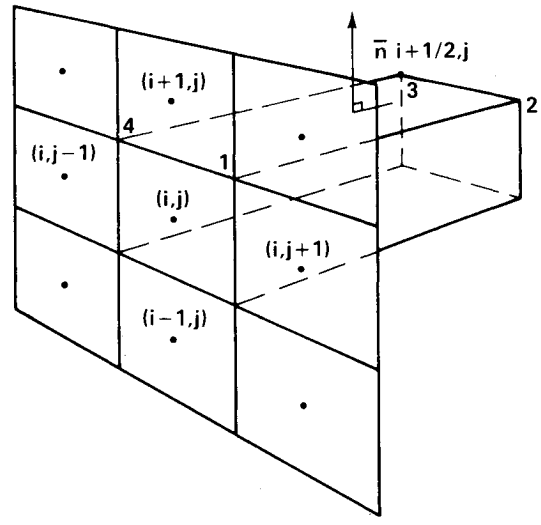

Fig. 4 Control volume nomenclature.

With M^* known, the remaining properties along θ follow immediately from the isentropic relations.

Numerical Scheme

Using the notation of Fig. 4, control volume mass and momentum conservation equations are given by

$$\boldsymbol{U}_{i,j}^{n+1} = \boldsymbol{U}_{i,j}^n - \boldsymbol{F}_{i+1/2,j} + \boldsymbol{F}_{i-1/2,j} - \boldsymbol{F}_{i,j+1/2} + \boldsymbol{F}_{i,j-1/2} \tag{6}$$

where

$$\boldsymbol{U}_{i,j}^n = A_{i,j}^n \begin{bmatrix} \rho w \\ \rho w^2 + p \\ \rho w u \\ \rho w v \end{bmatrix}_{ij} \boldsymbol{F}_{i+1/2,j} = \begin{bmatrix} \rho V \\ \rho w V + n_z p \\ \rho u V + n_x p \\ \rho v V + n_y p \end{bmatrix}_{i+1/2,j}$$

$$V = \boldsymbol{n}_{i+1/2,\cdot,j} \cdot (u, v, w)_{i+1/2,j} \tag{7}$$

Equations (6) are closed using the constant total enthalpy condition and the perfect-gas equations of state that yield the constraint

$$\frac{p}{\rho} \frac{\gamma}{(\gamma - 1)} + \frac{1}{2}(u^2 + v^2 + w^2) = H_0 \tag{8}$$

To advance Eqs. (6), it is necessary to evaluate the fluxes F at the edges of the control volume. Godunov's method uses the Riemann problem to estimate cell edge properties. A marching step is completed as follows:

1) The step size is computed using the CFL condition and the coordinates of the control volume corners are determined. The vector normal to each cell edge is calculated from

$$\boldsymbol{n} = \tfrac{1}{2}(\boldsymbol{v}_{24} \times \boldsymbol{v}_{31})$$

where $\boldsymbol{v}_{ij} = (x_i - x_j, y_i - y_j, z_i - z_j)$ and the subscripts refer to the corner numbers, which for edge $(i+1/2, j)$ are defined in Fig. 4.[12]

2) A Riemann problem is constructed for each cell edge using the two adjacent cell properties. The two dimensions associated with it are defined by plane R, which contains the cell edge normal vector and is aligned with the z axis. The two initial states consist of (p, ρ, v_n, w) at the two adjacent cells, where $v_n = (un_x + vn_y)/|(n_x, n_y)|$. Also computed for each initial state is $v_t = (-un_y + vn_x)/|(n_x, n_y)|$, which is the

velocity component tangent to the cell edge trace in the $z=z^n$ plane.

3) The Riemann problem associated with each edge is solved using the technique described previously.

4) The angular orientation of the cell edge is plane R is calculated. With respect to edge $(i+\frac{1}{2},j)$, this orientation is given by

$$\theta=\tan^{-1}\left[-\frac{n_{z_{i+\frac{1}{2},j}}}{(n^2_{x_{i+\frac{1}{2},j}}+n^2_{y_{i+\frac{1}{2},j}})^{\frac{1}{2}}}\right] \tag{9}$$

5) Estimated cell edge properties are constructed using the Riemann solution values of p,ρ,v_n,w along θ and by assigning a tangential velocity component value v_t that is selected by noting the relation between θ and the Riemann solution slip line direction δ_f. On edge $(i+\frac{1}{2},j)$, for example,

$$v_t=\begin{cases} v_{t_{i+1,j}} & \text{if } \theta\geq\delta_f \\ v_{t_{i,j}} & \text{if } \theta<\delta_f \end{cases} \tag{10}$$

Note that δ_f is the flow direction in plane R and is defined by $\delta_f=\tan^{-1}(v_n/w)$.

6) Once the edge property values have been obtained on each of the four edges, the required fluxes are evaluated using Eqs. (7) and Eqs. (6) are then advanced. The computational step is completed by decoding U to determine p,ρ,u,v, and w.

Boundary Conditions

The inviscid boundary conditions require that the velocity vector at a surface be tangent to the surface. Along edges abutting a surface, this implies that $V=0$ in Eq. (7) and that the flux is a function of pressure only. The pressure at the wall is determined by applying either a shock or expansion to property values of the cell adjacent to the wall. The appropriate shock or expansion is the one producing a final velocity vector parallel to the wall. This procedure is a natural reduction of the Riemann problem to the situation where the final streamline direction is known.

The wall pressure predicted by the above procedure is used to advance the solution. However, these values are only locally first order in smooth flow regions and a more accurate surface pressure estimate is needed for evaluating aerodynamic coefficients. This is accomplished using the reference plane method of characteristics to predict the pressure at the center of the cell edge abutting the wall. On plane R, the reference plane characteristic equation applicable along $\delta\pm\mu$ has the form

$$p_w-p_c\pm\kappa_\pm(\delta_w-\delta_c)=S \tag{11}$$

Here the right-hand side contains derivatives normal to plane and the upper sign is applied along the $\delta+\mu$ characteristic. To determine p_c at $z=z^n+\Delta z/2$ directly, the characteristic intersecting the wall from the flow interior is used, S is the explicitly evaluated at $z=z^n$, δ is the known wall slope, and (p_c,δ_c) are determined by interpolation. Here (p_c,δ_c) are evaluated at the point where the characteristics in R plane passing through the cell edge center intersects $z=z^n$. To promote robustness, this procedure is approximated in two steps:

$$\tilde{p}=\begin{cases} \text{Eq. (2) if } \pm(\delta_w-\delta_\pm)<0 \\ \text{Eq. (3) otherwise} \end{cases} \tag{12a}$$

$$p_w=\tilde{p}+S \tag{12b}$$

Furthermore, derivatives are determined using a limiting procedure similar to that of Ref. 1. In smooth-flow regions, derivatives are of second order, Eq. (12a) reduces to Eq. (4), and Eqs. (12) in combination are equivalent to Eq. (11). Near large gradients, limiting reduces the derivatives to zero and the first-order boundary condition, consisting of a shock or an expansion, is recovered.

As the solution is marched down the length of a missile, lifting surfaces may be encountered in one step which were not present in the previous step and vice versa. This can led to element edges that are only partly covered by a surface. Such edges are divided into two sections: one containing the edge area adjacent to the surface, and the other the edge area adjoining another element. Separate estimates are made of the fluxes acting on each section and these are added to determine the total edge flux.

The outer zone boundary (i.e., edge 3 in Fig. 2) is determined by tracking the domain of dependence using the information contained in the Riemann solution. Prior to the execution of each step, a Riemann problem is constructed for each cell edge abutting the freestream. The initial states for this problem are the freestream conditions and the abutting cell properties. The Riemann solution features a direction θ that

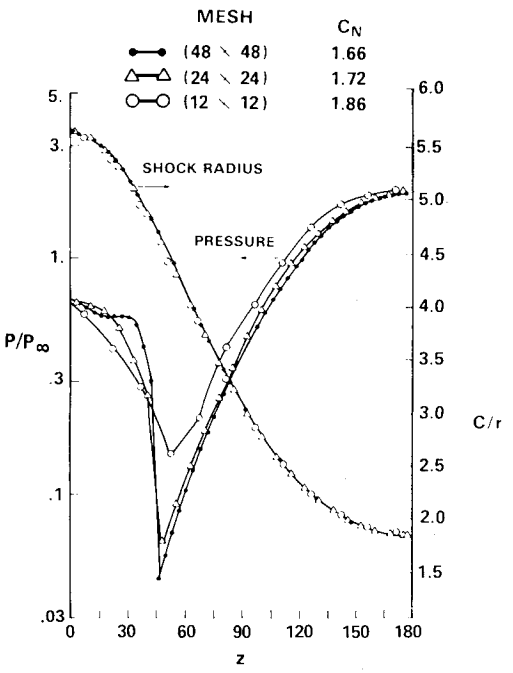

Fig. 5 Calculated cross-flow surface pressure and shock shape on a tangent-ogive with nose fineness of 2.5 using three different meshes at $z=8.50$.

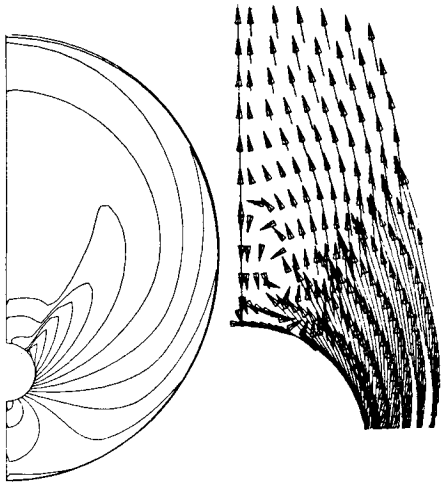

Fig. 6 Calculated cross-flow velocities and pressure contours on a tangent-ogive with nose fineness of 2.5 using the 48×48 mesh at $z=8.50$.

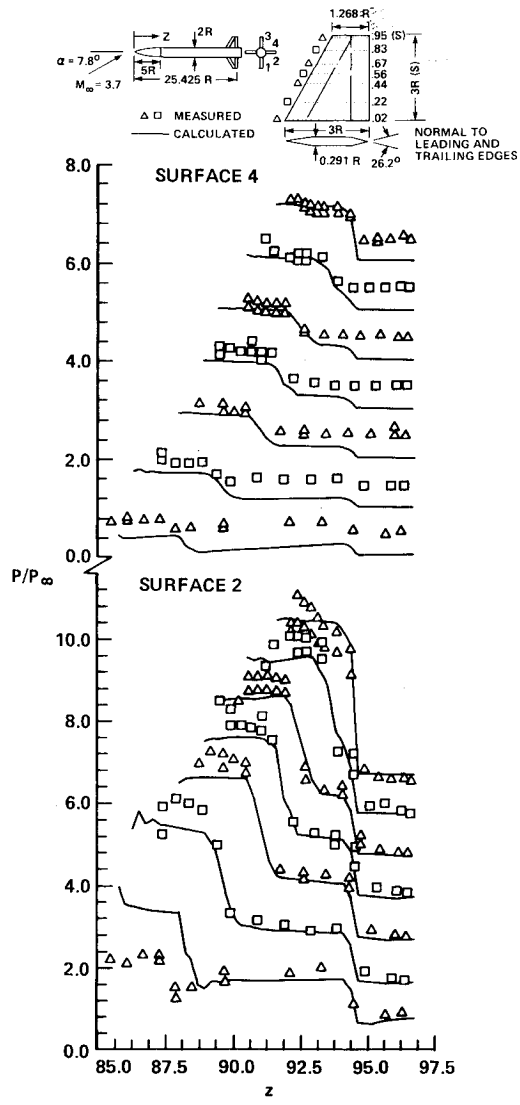

Fig. 7 Calculated and measured fin surface pressure on the clipped delta fin configuration of Ref. 14. Reference zero shifted by 1.0 for each successive curve.

separates the freestream flow from other states. This angle marks the edge of the domain of dependence of the numerical solution in plane R. The outer edge of the cell abutting the freestream is defined such that its trace in plane R is in the direction θ.

Results

Godunov's method has been applied to body-alone as well as body/wing configurations. In all cases, the missile nose was taken as sharp and the initial data plane was defined a short distance from the nose tip using the approximate conical flowfield generator of Ref. 14. The solution was generally advanced at 90% of the CFL step size and, thus, it was not necessary to apply either special procedures or artificial viscosity. Near the fin leading edges, where large pressure jumps occurred, small surface pressure oscillations were reduced by using a smaller step size (e.g., 50% of the CFL limit).

Figure 5 illustrates calculated surface pressure and shock shape on a tangent ogive body, with a nose fineness of 2.5 at Mach 3.5 and an incidence of 15 deg. Results are provided for three different mesh sizes; the calculated normal force per unit length is also shown. For the purposes of calculating loads, the 24×24 mesh provides sufficient resolution. However, details of the flowfield structure are enhanced by the 48×48 mesh. The surface pressure profiles indicate the presence of a crossflow shock on the leeside of the body, whose description is sharpened as the mesh is refined. Figure 6 illustrates the crossflow plane, generated by the 48×48 mesh, which features a small vortex on the leeside of the model. This vortex is produced by the crossflow shock and is not evident in the 24×24 mesh results.

Calculated surface pressures are shown in Fig. 7 for a cruciform, cranked delta configuration in the plus-roll orientation. Experimental data are from Ref. 15 and were measured at a Mach number of 3.7, an incidence of 7.8 deg, and Reynolds number based on a diameter of 1.8×10^5. For these conditions, attached shocks or expansions occurred at the fin leading edges. The calculation was started near the nose tip using a 12×12 mesh that was regrid at $z=2$ and 5 to 15×18 and 18×24, respectively. The final section containing the fins extended from $z=80$–102 and was run using a 36×36 mesh and 50% of the allowable CFL step size. The calculated surface pressure agrees well with experiment over most of the fin surface. The cross-flow velocity vectors and pressure contours at

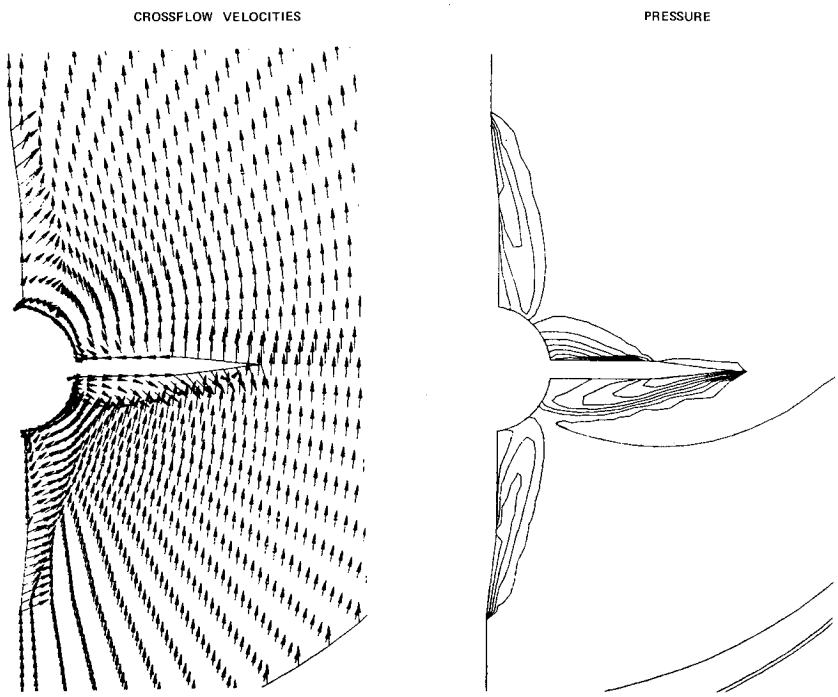

Fig. 8 Computed cross-flow velocities and pressure contours at $z=96.5$ on the configuration of Fig. 8.

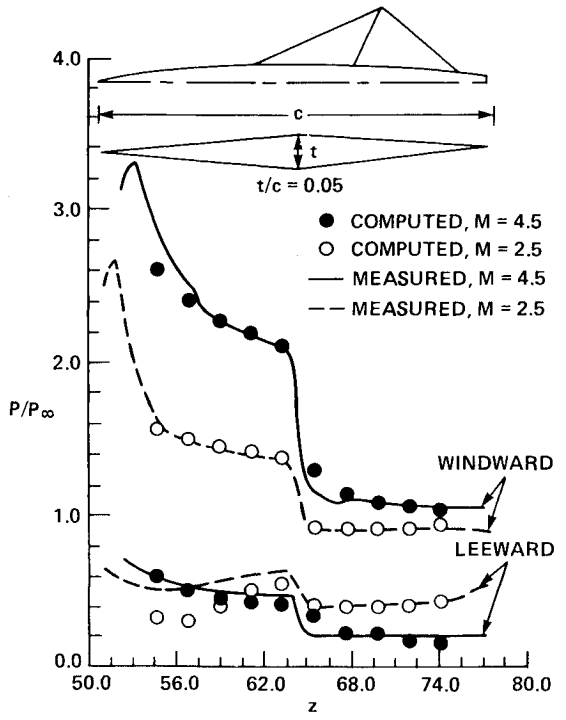

Fig. 9 Calculated and measured wing surface pressures on the swept wing model of Ref. 15 at $\alpha = 6$ deg.

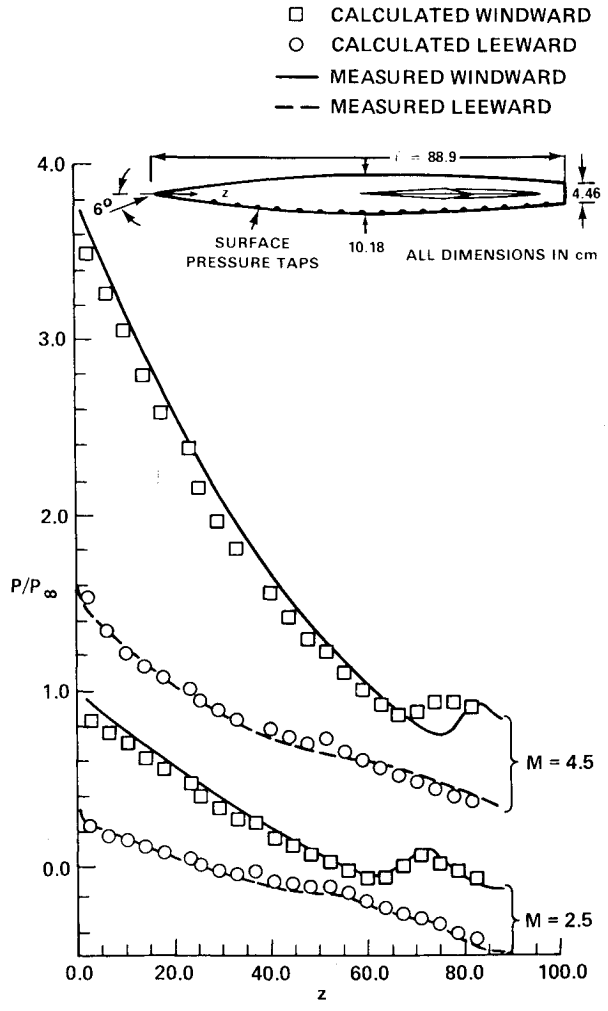

Fig. 10 Calculated and measured body surface pressures on the swept wing model of Ref. 15 at $\alpha = 6$ deg.

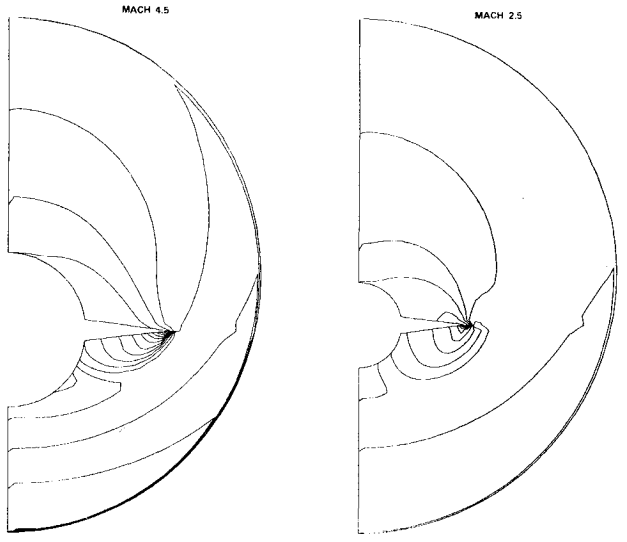

Fig. 11 Computed pressure contours on the configuration of Fig. 9 at a station slightly forward of the wing tip.

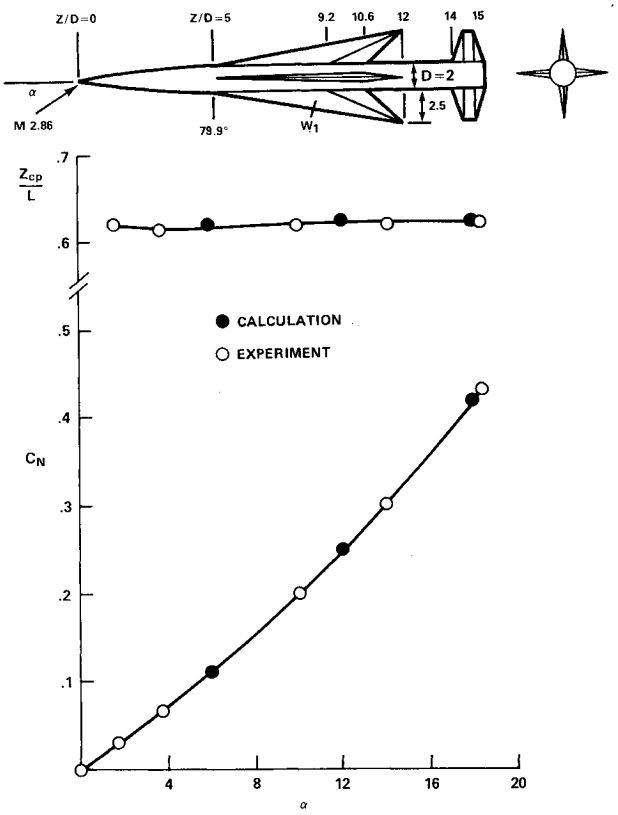

Fig. 12 Calculated and measured normal force and center of pressure on the body/wing/tail model of Ref. 16.

an axial station near the fin midcord are given in Fig. 8. Shocks can be seen attached to the fin edges.

Calculations have been performed on the swept wing configuration (tested in Ref. 16) shown in Fig. 9, which was run at an incidence of 6 deg and Mach numbers of 2.5 and 4.5. A 14×18 mesh was applied forward of the wing and a 36×36 mesh was used for the remainder of the body. The step size was reduced to 66% of the allowable CFL limit over the wing portion of the body. Calculated and measured wing surface pressures are shown in Fig. 9 and agree well in most cases. However, near the wing leading edge, computed values are

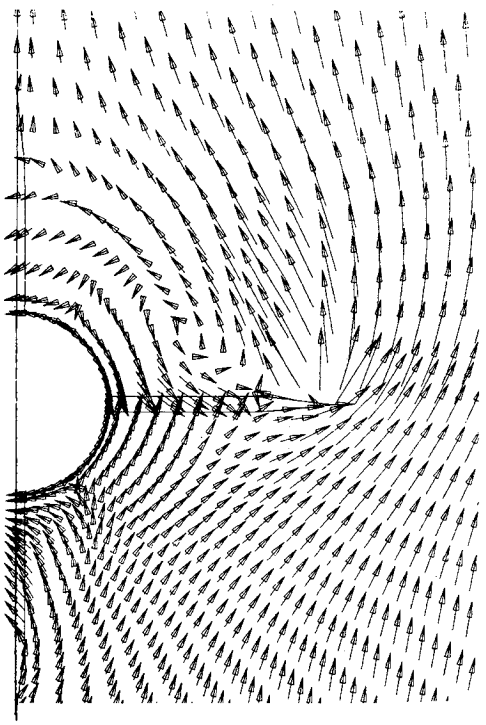

Fig. 13 Cross-flow velocity on the model of Fig. 12 at $z = 11.80$.

larger than measured ones. Figure 10 provides measured and calculated surface pressures on the windward and leeward sides of the body. Calculated windward pressures are slightly larger than measured ones and the calculated jump in pressure due to the wing occurs further aft than the measured one at Mach 4.5. Computed leeside pressures agree well with measured ones. The cross-flow pressure contours are shown in Fig. 11 at an axial station slightly upstream of the wing tip at Mach 2.5 and 4.5. A detached shock is visible below both wings and, at the higher Mach number, it is positioned closer to the wing surface. This produces the strong wing surface pressure gradients visible at this Mach number in Fig. 9. At Mach 4.5, the Mach number to the leading edge is supersonic, but is not large enough to produce an attached shock that could turn the flow in the plane of the lower wing surface.

The final case considered is the wing/body/tail configuration of Ref. 17 which is shown in Fig. 12. Here, the highly swept wing features a leading-edge normal Mach number that is subsonic. A 15×18 mesh was used forward of the wing and a 36×36 mesh was applied over the remainder of the body. The computed normal force and center of pressure are given in Fig. 12 and agree well with experiment. The computed cross flowfield at an axial station near the wing trailing edge is shown in Fig. 13 and features a leeside vortex that is convected over the tail.

Conclusions

A Godunov method for tactical missile shapes in supersonic flow has been developed and applied to several different tactical missiles. This scheme uses a multiple-zone approach to generate a grid for finned tactical missiles. It is cast in a finite-volume framework and fits the bow shock using the information contained in the Riemann problem. A postprocessing technique based on the method of characteristics is used to improve estimates of the surface pressure. Results have been applied to several different missiles, with and without fins, and satisfactory agreement has been obtained with measurement. It was not necessary in any of these cases to use special procedures or artificial viscosity.

The merits of Godunov's scheme can be illustrated by comparing it with the finite-difference method of Ref. 9. Here a similar multiple-zone mesh generation scheme is applied in conjuction with MacCormack's second-order explicit scheme and calculations are completed on many of the same shapes. The principle advantage of Godunov's scheme is its robustness, which allows complicated cases to be completed without user intervention or application of special procedures. For example, computation of the body/wing/tail configuration shown in Fig. 12 using the method of Ref. 9 required fine tuning of the artificial viscosity coefficients as well as careful selection of the fin edge differencing option, while Godunov's method handled this configurations without any adjustments. In regions of the flow featuring strong shocks or expansions (e.g., on fins), the accuracy of the Godunov method appears comparable to that of Ref. 9. However, in smooth flow regions, Godunov's method is first-order accurate and therefore less accurate. For example, using the method of Ref. 9 and a mesh size comparable to that employed in this paper, the body surface pressures forward of the wing in Fig. 10 are more accurately resolved. Furthermore, the required computational time per mesh point per step is twice as large for Godunov's method as currently implemented. However, the robust behavior of the Godunov scheme makes it accessible to the casual user and the lack of cumbersome special procedures allows it to be extended to handle arbitrarily complex configurations.

Acknowledgments

This work was supported by NSWC I.R., NAVSEA, and NAVAIR. The project monitors were Dale Hutchins (AIR-310-C) and Lionel Pasiuk (SEA-62R41).

References

[1]Glaz, H.M. and Wardlaw, A.B., "A High-Order Godunov Scheme for Steady Supersonic Gas Dynamics," *Journal of Computational Physics,* Vol. 58, April 1985, pp. 157–187.

[2]Thomas, P.D., Vinokur, M., Bastianon, R., and Conti, R.J., "Numerical Solution for Three-Dimensional Inviscid Supersonic Flow," *AIAA Journal,* Vol. 10, July 1972, pp. 887–894.

[3]Moretti, G., Grossman, B., and Marconi, F., "A Complete Numerical Technique for the Calculation of Three-Dimensional Inviscid Supersonic Flow," AIAA Paper 72-192, 1972.

[4]Marconi, F. and Salas, M., "Computation of Three Dimensional Flows About Aircraft Conigurations," *Computers and Fluids,* Vol. 1, 1973, pp. 185–195.

[5]Kutler, P., Reinhardt, W.A., and Warming, R.F., "Multishocked, Three-Dimensional Supersonic Flowfields with Real Gas Effects," *AIAA Journal,* Vol. 11, May 1973, pp. 657–664.

[6]Kyriss, C.L. and Harris, T.B., "A Three-Dimensional Flow Field Computer Program for Maneuvering and Ballistic Re-entry Vehicles," Paper presented at Tenth U.S. Navy Symposium on Aeroballistics, July 1975.

[7]Marconi, F., Salas, M., and Yeager, L., "Development of a Computer Code for Calculating th Steady Super/Hypersonic Inviscid Flow around Real Configurations, Vol. 1—Computational Techniques," NASA CR 2675, April 1976.

[8]Moretti, G., "Conformal Mappings for Computation of Steady, Three-Dimensional, Supersonic Flows," *Numerical/Laboratory Computer Methods in Fluid Dynamics,* No. 13, ASME, New York, 1976.

[9]Wardlaw, A.B., Baltakis, F.P., Solomon, J.M., and Hackerman, L.B., "An Inviscid Computational Method for Tactical Missile Configurations," NSWC TR 81-457, Dec. 1981.

[10]Wardlaw, A.B., Priolo, F.J., Solomon, J.M., and Baltakis, F.P., "Inviscid Multiple Zone Calculations for Supersonic Tactical Missiles," AIAA Paper 84-2099, Aug. 1984.

[11]"Equations, Tables and Charts for Compressible Flow," NACA 1135, 1953.

[12]Kordulla, W. and Vinokur, M., "Efficient Computation of Volume in Flow Predictions," *AIAA Journal,* Vol. 21, June 1983, p. 917.

[13]Wardlaw, A.B. Jr., Baltakis, F.P., Martin, F.M., Priolo, R.G., and Jettmar, R.U., "Godunov's Method for Supersonic Tactical Missile Computations," AIAA Paper 85-1813, 1985.

[14]Wardlaw, A.B., Hackerman, L.B., and Baltakis, F.P., "An Inviscid Computational Method for Supersonic Missile Type Bodies—Program Description and Users Guide," NSWC TR 81-459, Dec. 1981.

[15]Lamb, M., Sawyer, W.B., Wassum, D.L., and Babb, C.D., "Pressure Distribution on Three Different Cruciform Aft-Tail Control Surfaces of a Wingless Missile at Mach 1.6, 2.36, and 3.78," Vols. II and III, NASA TM 80097, Aug. 1979.

[16]Jackson, C.M. Jr. and Sawyer, W.C., "A Method for Calculating the Aerodynamic Loading on Wing Body Combinations at Small Angles of Attack in Supersonic Flow," NASA TN D-6441, 1971.

[17]Spearman, M.L. and Swayer, W.C., "Longitudinal Aerodynamic Characteristics at Mach Numbers from 1.6 to 2.86 for a Fixed-Span Missile with Three Wing Planforms," NASA TM 74088, Nov. 1977.